

pubs.acs.org/acscatalysis Research Article

# Cleavage of C-O and C-C Bonds in Lignin-Derived Compounds to Produce Aromatics Using Molybdenum-Containing MFI Zeolites

Jie Zhu, Matthew S. Webber, Jamison Watson, Gregg T. Beckham,\* and Yuriy Román-Leshkov\*



Cite This: ACS Catal. 2025, 15, 14782-14793



**ACCESS** I

III Metrics & More

Article Recommendations

Supporting Information

ABSTRACT: Lignin, the most abundant source of renewable arenes, is a viable feedstock for the production of aromatic compounds. However, the prevalence of resilient C–C bonded oligomeric fragments in lignin-derived streams can compromise monomer yields during reductive catalytic fractionation (RCF). To address this issue, we developed a bifunctional molybdenum-containing MFI (Mo/H-MFI) zeolite catalyst capable of cleaving both C–O and C–C bonds in lignin-derived molecules to produce aromatic monomers. Using propylguaiacol as a model compound, we demonstrated the importance of proximity between metallic molybdenum carbide sites and the Brønsted acid sites in the zeolite in achieving high carbon yields (~80%) of benzene, toluene,



propylbenzene, and phenol while maintaining catalyst stability (>98% stable conversion for 20 h). A reaction network involving both C–O and C–C bond cleavage pathways was proposed based on kinetic studies using key intermediates as feeds. Finally, we successfully depolymerized partially deoxygenated lignin oil obtained from the RCF of poplar using a continuous, two-pass catalytic process. This work highlights the potential of the bifunctional Mo/H-MFI catalyst in upgrading complex lignin feedstocks and provides a methodological approach for converting lignin-derived compounds into platform aromatic chemicals.

KEYWORDS: lignin, hydrodeoxygenation, C-C bond cleavage, platform aromatics, molybdenum-containing MFI zeolites

#### 1. INTRODUCTION

Lignin, constituting 15–30 wt % of lignocellulosic biomass, comprises methoxylated phenylpropanoid subunits connected by C–C and C–O bonds. <sup>1–3</sup> Given the increasing demand for platform aromatics like benzene, toluene, xylene (BTX), and phenol, transforming lignin-derived compounds into these high-value building blocks represents a promising avenue for lignin valorization. <sup>1,2,4–12</sup> However, breaking the C–C and C–O bonds in lignin efficiently while maintaining both aromaticity and high carbon yields remains a major challenge. <sup>3,5,10,13,14</sup>

Catalytic hydrodeoxygenation (HDO) relies on direct hydrogenolysis or tandem hydrogenation/dehydration sequences to cleave aryl C-O bonds. 15-24 Noble metal-based catalysts, such as Pt, Rh, Pd/C, and Ru/Al<sub>2</sub>O<sub>3</sub>, exhibit high HDO activity of lignin-derived compounds; however, they often saturate the aromatic ring, thereby limiting the yield of the desired aromatic products. 15,25-27 In parallel, metal sulfide (e.g., NiMoS<sub>2</sub>, CoMoS<sub>2</sub>) and phosphide (e.g., Ni<sub>2</sub>P, Fe<sub>2</sub>P, and NiMoP) catalysts have also shown promising HDO performance. Recent studies have reported notable improvements in the stability and activity of these catalysts, mitigating some of the long-standing challenges such as sulfur and phosphorus leaching. However, despite these improvements, trace leaching of active elements still remains a concern, particularly

in applications requiring high product purity. Moreover, many of these systems exhibit limited aromatic selectivity. Amid these developments, molybdenum carbide ( $Mo_2C$ ) stands out as a robust, earth-abundant catalyst capable of selective C–O bond hydrogenolysis without substantial aromatic ring saturation. <sup>36–40</sup>

While significant research has focused on cleaving C–O bonds in lignin-derived molecules, comparatively less emphasis has been given to C–C bond cleavage. Besides having a higher dissociation energy, efficient C–C bond cleavage faces additional challenges, including steric hindrance between functional groups and the complex evolution of surface species. Several strategies can be implemented to cleave the interunit C–C bonds in lignin-derived molecules. Dealkylation of monomeric lignin compounds was demonstrated using acidic catalysts, such as phosphate-based materials, NbO<sub>x</sub>-supported catalysts, and zeolite catalysts. S,22,44,51,52 Zeolite-based catalysts, in particular, showed

Received: April 4, 2025 Revised: June 24, 2025 Accepted: July 21, 2025



high selectivity for removing the propyl chain from deoxygenated monolignols to generate phenol and benzene. 5,8,53-55 As a result, bifunctional metal-containing zeolites, which combine the advantages of metallic and acidic species, have emerged as promising catalysts for the tandem cleavage of both C-O and C-C bonds. 14,55-57 However, these catalytic systems, which primarily operate in batch mode, often rely on expensive noble metals and tend to result in hydrogenated products during HDO. Accordingly, practical lignin conversion to BTX necessitates the development of robust, nonprecious metal-based catalysts capable of simultaneously removing methoxy, phenolic hydroxy, and alkyl chains from guaiacyl and syringyl monomers without saturating the aromatic ring.

Herein, we developed Mo-containing MFI zeolites as bifunctional catalysts to continuously generate platform monoaromatics (e.g., benzene, toluene, propylbenzene, and phenol) through selective C-O and C-C bond cleavage in lignin-derived molecules. Using propylguaiacol as a model compound, we examined the synergistic effects between metallic and Brønsted acid sites to cleave C-C and C-O bonds. The spatial proximity between these sites was an important parameter for both obtaining high selectivity (>90%) toward target aromatic products and enhancing catalyst stability with over 98% stable conversion for 20 h. Acid sites facilitated alkyl chain removal from the aromatic ring, with increased zeolite acidity promoting product methylation. A reaction network involving both C-O and C-C bond-breaking pathways was built from kinetic studies using intermediate compounds. By applying the same catalyst system to both model compounds and real lignin-derived phenolic mixtures, we demonstrated that the mechanistic insights from simplified models can effectively guide the valorization of complex lignin feedstocks, bridging the gap between fundamental studies and practical application. To this end, we developed a continuous, dual-pass catalytic process for upgrading real lignin-derived bio-oil, which achieved improved yields of monoaromatic products via C-C bond cleavage of lignin oligomers and offered significant advantages over conventional batch processing techniques.

# 2. RESULTS AND DISCUSSION

2.1. Synergistic Effect between Metallic Mo<sub>2</sub>C and **Brønsted Acid Sites.** We investigated the cleavage of C-O and C-C bonds using propylguaiacol (2-methoxy-4-propylphenol) as a model compound where the aromatic ring contains the three typical functional groups commonly present in lignin-derived monomers: methoxy ( $C_{sp2}$ –OCH<sub>3</sub>), hydroxyl ( $C_{sp2}$ –OH), and propyl ( $C_{sp2}$ – $C_{sp3}$ ) groups. Bulk  $Mo_2C$ (Figures 1A and S1, S2) was first tested as a control for the vapor-phase HDO of propylguaiacol at 350 °C under ambient H<sub>2</sub> pressure. As shown in Figure 1B, the conversion of propylguaiacol using the Mo<sub>2</sub>C catalyst reached 80% and then declined to 20% over a 20 h time frame. Initially, Mo<sub>2</sub>C primarily generated propylbenzene by cleaving both methoxy and phenolic groups. However, as the catalyst deactivated, propylphenol became the dominant product (Figure 1C). The observed shift in product selectivity from propylbenzene (80% initially) to propylphenol (92% after 20 h) suggests that  $Mo_2C$  preferentially cleaves the  $C_{\rm sp2}-OCH_3$  bond in propylguaiacol before the C<sub>sp2</sub>-OH bond, in agreement with prior studies. <sup>58,59</sup> Indeed, the decrease in C-O bond cleavage efficiency is attributed to the oxidation of Mo<sub>2</sub>C by oxygenated lignin-derived compounds, resulting in the formation of

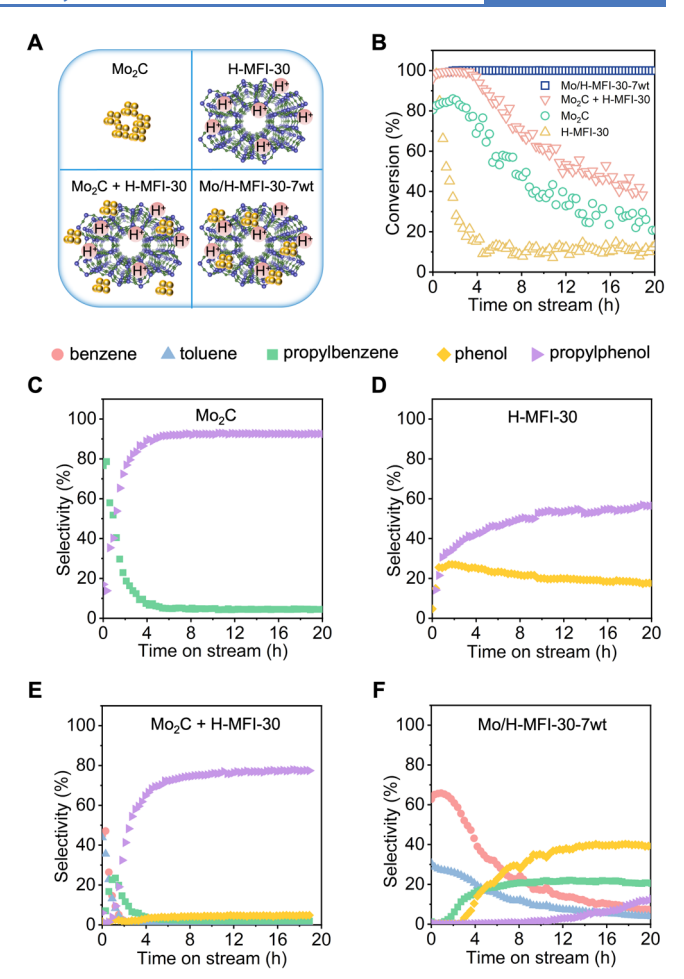


**Figure 1.** (A) Illustration of bulk Mo<sub>2</sub>C, H-MFI-30, a physical mixture of Mo<sub>2</sub>C + H-MFI-30 and Mo/H-MFI-30-7wt catalysts. (B) Conversion time profile and (C–F) product selectivity of propylguaiacol HDO over different catalysts. Reaction conditions: (C) 0.022 g Mo<sub>2</sub>C, (D) 0.3 g H-MFI-30, (E) 0.022 g Mo<sub>2</sub>C + 0.3 g H-MFI-30, and (F) 0.3 g of Mo/H-MFI-30-7wt; diluted with SiC to yield a 2 g mixture, 350 °C, 150  $\mu$ L/h propylguaiacol, and 70 mL/min H<sub>2</sub>.

molybdenum oxycarbide species.<sup>60,61</sup> Notably, minimal C–C bond cleavage was observed with the Mo<sub>2</sub>C catalyst alone.

An H-MFI zeolite with a Si/Al ratio of 30 (H-MFI-30), known for its dealkylation and cracking activity, was used to cleave the alkyl group in propylguaiacol. 5,44,53,55,62 The production of phenol after reaching steady state confirmed C-C bond cleavage by the H-MFI-30 catalyst (Figure 1D). Moreover, the presence of propylphenol (60% after 20 h) indicated acid-catalyzed demethoxylation activity. Notably, physically mixing Mo<sub>2</sub>C with H-MFI-30 (in equal proportions as when using each catalyst separately) enhanced the observed reactivity. Initially, aromatic products such as benzene, toluene, and propylbenzene were detected, although their selectivity rapidly decreased (Figure 1E). After 2 h on-stream, propylphenol predominated with minimal phenol presence. These results suggest that the Mo<sub>2</sub>C + H-MFI-30 physical mixture can activate both C-O and C-C bonds, and the proximity between the Mo<sub>2</sub>C and the Brønsted acid sites in H-MFI-30 appears to facilitate tandem deoxygenation and dealkylation reactions.

To investigate the impact of site proximity on catalyst performance, we synthesized a Mo-incorporated MFI zeolite

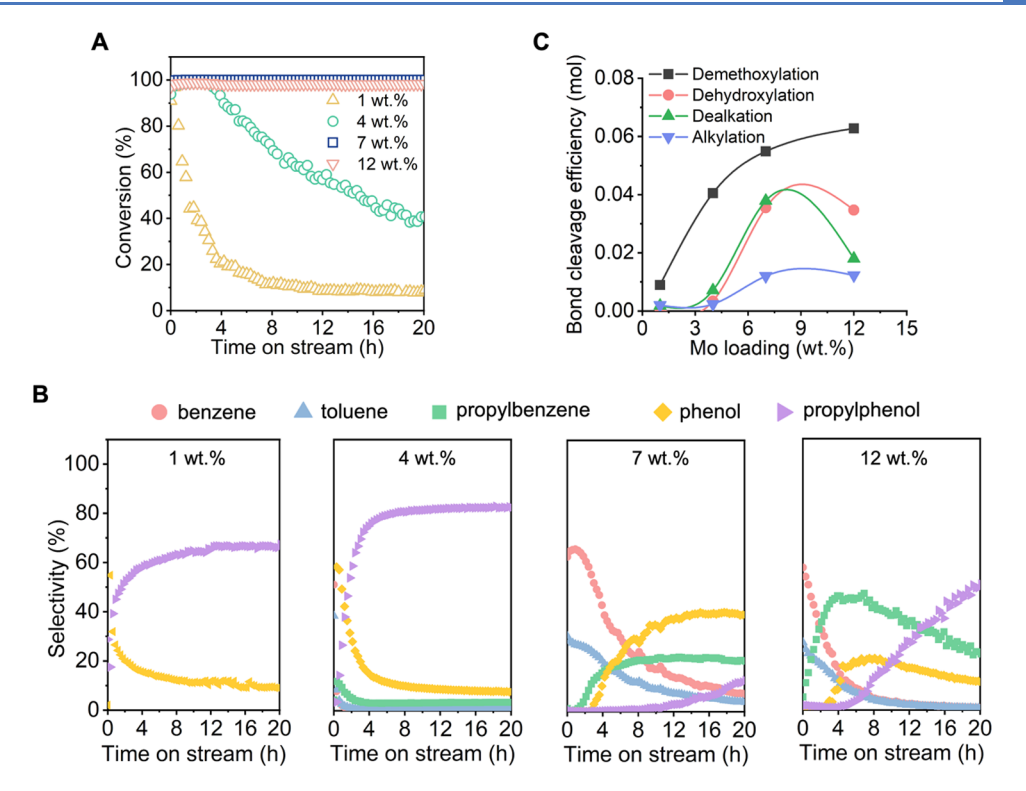
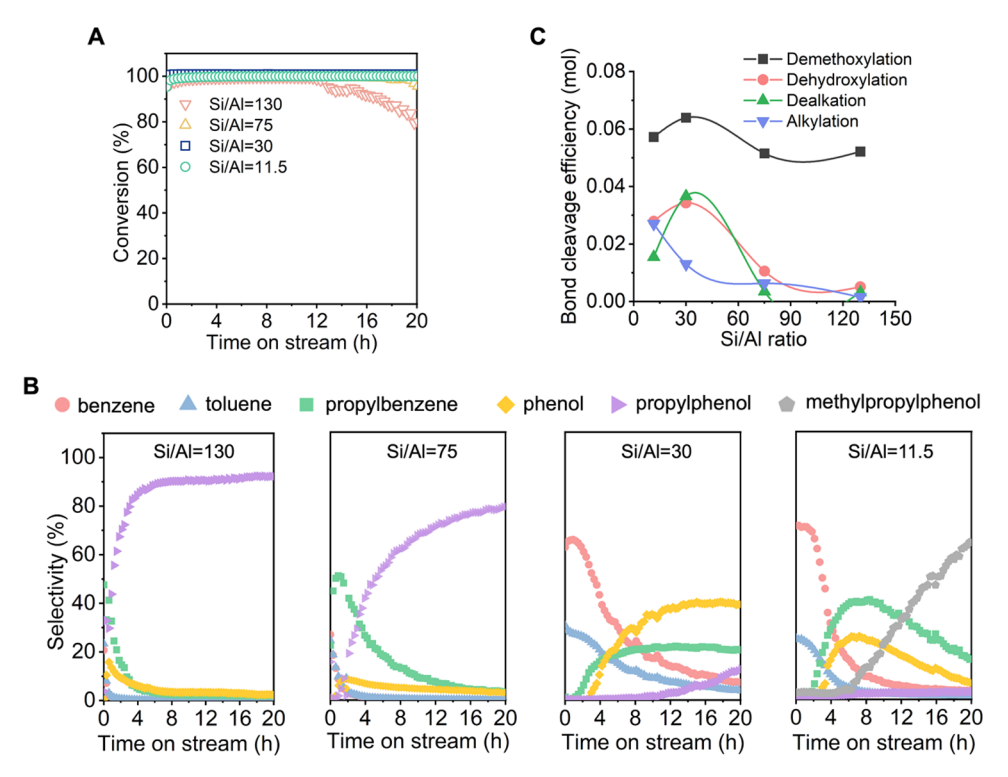


Figure 2. (A) Conversion time profile of Mo/H-MFI-30-*x* catalysts with different molybdenum loadings. (B) Product selectivity of propylguaiacol HDO over Mo/H-MFI-30-*x* catalysts. (C) Efficiency of bond cleavage over Mo/H-MFI-30-*x* catalysts. *x* denotes the molybdenum loading of the catalyst. The bond cleavage efficiency is calculated based on the mole of the formed products. Reaction conditions: 0.3 g of Mo/H-MFI-30-*x* diluted with 1.7 g SiC, 350 °C, 150 μL/h propylguaiacol, and 70 mL/min H<sub>2</sub>.

(Si/Al = 30) with a 7 wt % molybdenum loading, designated as Mo/H-MFI-30-7wt, via an impregnation method. PXRD patterns confirmed the MFI structure with high crystallinity (Figure S3). Mo/H-MFI-30-7wt showed a reduced micropore volume  $(0.09 \text{ cm}^3/\text{g})$ , compared to H-MFI-30  $(0.13 \text{ cm}^3/\text{g})$ (Figure S4), likely due to MoO<sub>3</sub> nanoparticle formation within the zeolite pores postcalcination. The TEM image of Mo/H-MFI-30-7wt (Figure S5) revealed a uniform MoO<sub>3</sub> particle distribution across the zeolite crystal, averaging approximately 1.3 nm. NH<sub>3</sub>-TPD profiles (Figure S6) showed a mixture of weak and strong acid sites in both H-MFI-30 and Mo/H-MFI-30-7wt, with Mo/H-MFI-30-7wt displaying a decrease in the proportion of strong Brønsted acid sites, indicative of MoO3 interaction with these sites. 63-65 After in situ carburization, Mo/H-MFI-30-7wt maintained high propylguaiacol conversion, exceeding 98% (Figure 1B), and produced a substantial amount of aromatics (i.e., benzene, toluene, propylbenzene, phenol) within the first 10 h (Figure 1F) on-stream. Despite having the same molybdenum loading as bulk Mo<sub>2</sub>C and the Mo<sub>2</sub>C + H-MFI-30 mixture, Mo/H-MFI-30-7wt showed superior propylguaiacol HDO activity. This contrast highlights the crucial role of Mo<sub>2</sub>C and Brønsted acid site proximity in cleaving both C-O and C-C bonds, facilitating the production of platform aromatics. Note that transalkylation by the zeolite support acid sites is likely responsible for alkylated product formation (Figure S7). TEM imaging of the spent Mo/H-MFI-30-7wt catalyst revealed that the high dispersion of molybdenum species was largely preserved after the reaction (Figure S8), suggesting no significant sintering occurred under the applied reaction conditions. After undergoing recalcination and recarburization, Mo/H-MFI-30-7wt maintained its high activity and selectivity in producing

platform aromatics, suggesting the feasibility of catalyst regeneration (Figure S9). Thermogravimetric analysis of spent catalysts (Figure S10) showed minimal coke formation ( $\sim$ 1 wt % weight loss) in both the mixture and impregnated Mo/H-MFI-30-7wt, indicating that catalyst deactivation may result from Mo<sub>2</sub>C oxidation, which leads to less effective bond cleavage.

2.2. Probing the Role of Metallic Mo<sub>2</sub>C and Brønsted Acid Sites for C-O and C-C Bond Cleavage. To elucidate the roles of the metallic Mo<sub>2</sub>C and the Brønsted acid sites in propylguaiacol HDO, we investigated Mo/H-MFI catalysts with varying molybdenum loadings and Si/Al ratios. These catalysts are denoted as "Mo/H-MFI-y-x," where "x" is the molybdenum loading and "y" is the Si/Al ratio. H<sub>2</sub>-TPR was employed to evaluate the reducibility of molybdenum species in Mo/H-MFI-30-x samples (x = 1wt, 4wt, 7wt, and 12wt). Two reduction peaks at 400-450 and 600-650 °C were observed for all catalysts, representing the reduction of MoO<sub>3</sub> to MoO<sub>2</sub> and aggregated MoO<sub>2</sub> species to metallic Mo, respectively (Figure S11). 66,67 The additional peak at 510 °C in Mo/H-MFI-30-7wt is likely associated with the reduction of MoO<sub>3</sub> species interacting with Brønsted acid sites. <sup>67,68</sup> Figure 2 shows the influence of molybdenum loading on activity and product distribution. The catalyst with the lowest molybdenum loading (1 wt %) showed similar performance to that of H-MFI-30, with rapid deactivation and products primarily consisting of propylphenol, phenol, methylpropylphenol, and methylphenol (Figures 2B and S12). At 4 wt % molybdenum loading, both higher propylguaiacol conversion and extensive C-C bond cleavage products were observed, suggesting that closer proximity between metal and acid sites may improve performance (Figure 2B). At 7 wt % loading, significant



**Figure 3.** (A) Conversion time profile of Mo/H-MFI-y-7wt catalysts with different acidities. (B) Product selectivity of propylguaiacol HDO over Mo/H-MFI-y-7wt catalysts. (C) Efficiency of bond cleavage over Mo/H-MFI-y-7wt catalysts. y denotes the Si/Al ratio of the catalyst. The bond cleavage efficiency is calculated based on the mole of the formed products. Reaction conditions: 0.3 g of Mo/H-MFI-y-7wt diluted with 1.7 g SiC, 350 °C, 150 μL/h propylguaiacol, and 70 mL/min H<sub>2</sub>.

hydrodeoxygenation and dealkylation activity were observed, generating mainly benzene, toluene, and propylbenzene. However, further increasing the molybdenum loading to 12 wt % led to a decline in benzene and toluene formation rates (Figure 2B). We attribute this effect to the sintering of  $Mo_2C$  nanoparticles during synthesis, as evidenced by TEM imaging of the catalyst prereaction (Figure S13). Despite less effective C–C bond cleavage compared to Mo/H-MFI-30-7wt, Mo/H-MFI-12wt maintained high HDO activity for the removal of methoxy and hydroxy groups. We surmise this product distribution results from the ample availability of  $Mo_2C$  sites in Mo/H-MFI-30-12wt, though with fewer of these sites positioned close to Brønsted acid sites to perform C–C bond cleavage chemistry.

To assess the impact that metallic Mo<sub>2</sub>C sites have on directing different reaction pathways, we measured bond cleavage efficiency as a function of products formed over the four catalysts. Specifically, demethoxylation efficiency was determined by summing the molar yields of products resulting from C<sub>sp2</sub>-OCH<sub>3</sub> removal, which includes benzene, toluene, propylbenzene, phenol, propylphenol, methylpropylbenzene, methylphenol, and methylpropylphenol. Similar calculations for dehydroxylation, dealkylation, and alkylation efficiencies were conducted, with results plotted as a function of molybdenum loading in Figure 2C. An increase in oxygencontaining group removal efficiencies, including demethoxylation and dehydroxylation, correlated positively with molybdenum loading. Contrarily, dealkylation efficiency peaked at 7 wt % molybdenum, and further increases in loading resulted in diminished C-C bond cleavage efficiency. These findings indicate that Mo<sub>2</sub>C species are critical for enabling C-O bond cleavage. An optimal molybdenum

loading is important for maximizing the proximity between  $Mo_2C$  and Brønsted acid sites, enhancing propyl side-chain cleavage.

To elucidate the effect of acidity on bond cleavage, four zeolite supports with varying Si/Al ratios were prepared. These materials were uniformly impregnated with 7 wt % molybdenum to synthesize Mo/H-MFI-y-7wt catalysts (y =11.5, 30, 75, and 130). PXRD patterns confirmed that all catalysts were crystalline (Figure S14). Their acidity was evaluated using NH3-TPD, showing increased NH3 uptake with decreasing Si/Al ratios (Figure S15), alongside a shift toward higher desorption temperatures for lower Si/Al ratios. H<sub>2</sub>-TPR profiles indicated that catalysts with increased acid density lower the reduction temperature of molybdenum species (Figure S16). Despite the varied levels of acidity, all catalysts showed high propylguaiacol conversion (Figure 3A). Catalysts with lower acid densities (i.e., Mo/H-MFI-130-7wt and Mo/H-MFI-75-7wt) predominantly yielded propylphenol and propylbenzene, with minor production of benzene, toluene, phenol, and methylated derivatives (Figures 3B and S17). A moderate acid density (Si/Al = 30) was optimal for breaking C-C bonds, while further increasing acidity enhanced the formation rates of methylated products, likely due to acid-catalyzed alkylation reactions (Figure 3B). These observations indicate that Brønsted acid sites are essential not only for facilitating alkyl chain removal but also for tuning product selectivity. A similar role of acidity was reported in prior work on MoO3-based catalysts for 4-propylguaiacol conversion, where more acidic supports promoted the formation of alkylated products.<sup>69</sup> Bond cleavage efficiencies over the four catalysts are summarized in Figure 3C. With constant molybdenum loading, all catalysts displayed com-

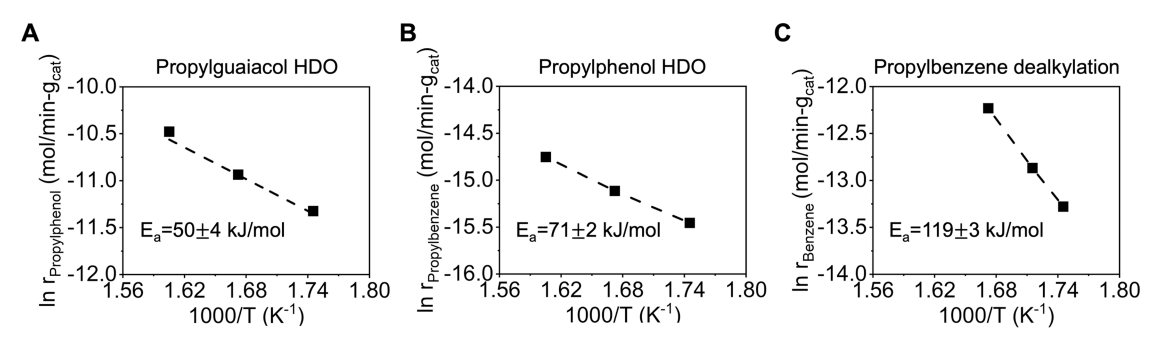
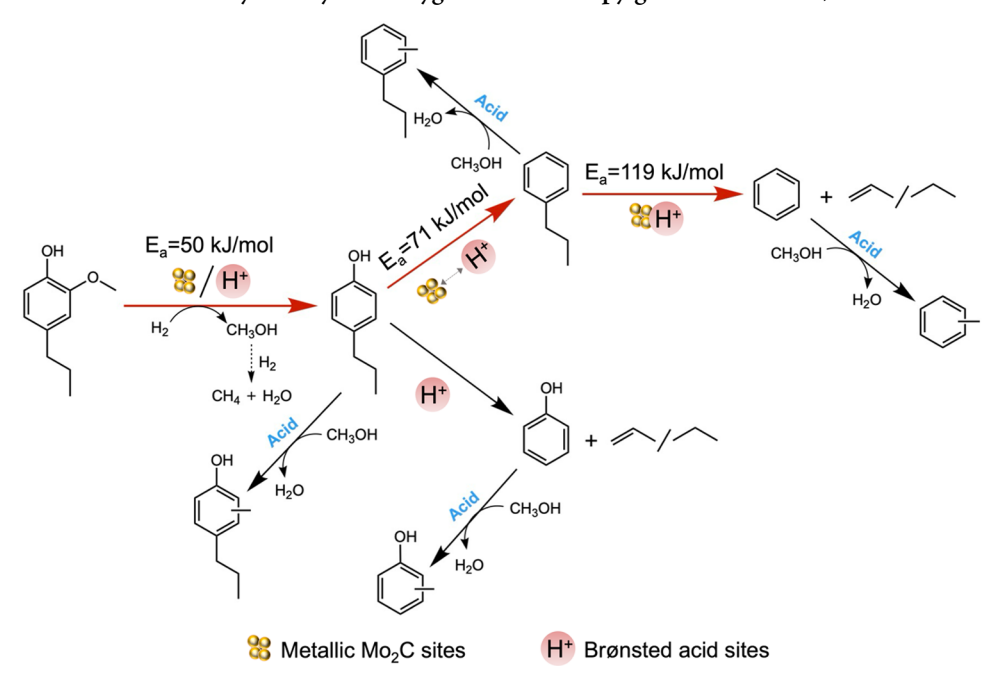


Figure 4. Kinetic studies for (A) propylguaiacol HDO, (B) propylphenol HDO, and (C) propylbenzene dealkylation over Mo/H-MFI-30-7wt. Reaction conditions: 0.03-0.04 g catalyst diluted with SiC, 300-350 °C,  $150 \mu$ L/h (A) propylguaiacol, (B) propylphenol, and (C) propylbenzene, and 70 mL/min H<sub>2</sub>, the substrate conversion was maintained at 10%.

Scheme 1. Proposed Reaction Pathway for Hydrodeoxygenation of Propylguaiacol over Mo/H-MFI-30-7wt



parable demethoxylation efficiencies, confirming that the molybdenum species play a central role in methoxy group removal. Peak dealkylation and dehydroxylation efficiencies were observed in the moderately acidic Mo/H-MFI-30-7wt sample, possibly due to an optimal metal-acid site ratio. These results highlight the need to balance the Mo<sub>2</sub>C sites and Brønsted acid sites proximity to efficiently cleave C–O and C–C bonds. The insufficient presence of either site reduces dealkylation and dehydroxylation efficiencies, resulting in only partially deoxygenated products.

2.3. Proposed Reaction Pathway for Propylguaiacol HDO. To further understand the propylguaiacol HDO reaction pathway, kinetic studies were conducted using the Mo/H-MFI-30-7wt catalyst under differential reaction conditions. Propylguaiacol and its intermediates, including propylphenol and propylbenzene, were used as feeds to identify primary, secondary, and tertiary products. These reactivity studies were performed at varying temperatures (300, 325, and 350 °C), ensuring substrate conversion remained at <10%. As shown in Figure S18A, propylguaiacol predominantly converted to propylphenol (~90%) through selective demethoxylation, with minor formation of propylbenzene and phenol. The formation rate of propylphenol as a function of temperature is

shown in Figure 4A, where the apparent activation energy for propylguaiacol demethoxylation was determined to be 50 kJ/ mol. This value is similar to the reported value (56 kJ/mol) for methoxy group removal from anisole. 70 Scheme 1 suggests that C<sub>sp2</sub>-OCH<sub>3</sub> bond cleavage is facilitated by either metallic Mo<sub>2</sub>C sites or Brønsted acid sites, given that propylphenol formation was observed across all catalysts regardless of their composition (Figure 1). The continuous formation of CH<sub>4</sub> and H<sub>2</sub>O throughout the reaction confirmed the fast hydrodeoxygenation of the methoxy group (Figure S19).71 When propylphenol was processed with the Mo/H-MFI-30-7wt catalyst, it underwent two parallel reactions: dehydroxylation to form propylbenzene and dealkylation to yield phenol (Figure S18B). The apparent activation energy for the dehydroxylation was 71 kJ/mol within the 300-350 °C temperature range (Figure 4B), demonstrating that this process is more demanding than methoxy group removal. The activation of the C<sub>sp2</sub>-OH bond necessitates both metallic and Brønsted acid sites (Scheme 1). The proportion of metal to acid sites influenced these reactions, affecting the selectivity of the final products (Figures 2 and 3). Lastly, using propylbenzene as a feed predominantly produced benzene (Figure S18C), where the activation energy for the alkyl group

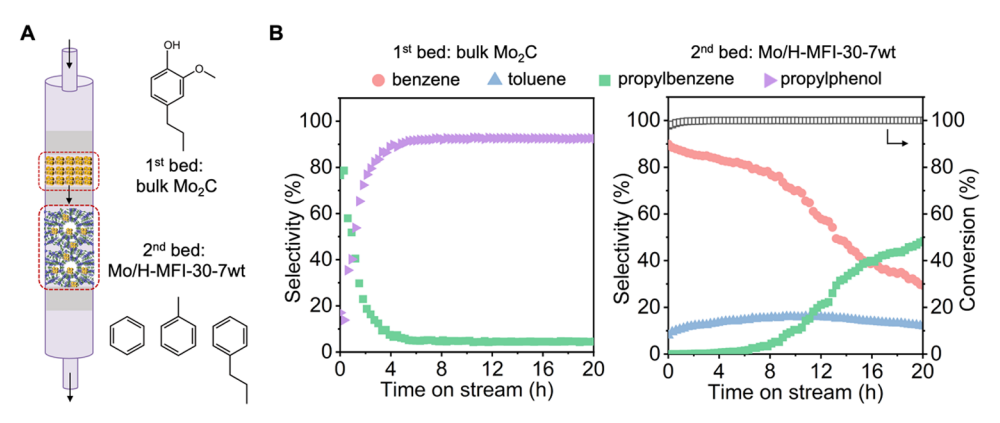


Figure 5. (A) Illustration of the dual-bed design for propylguaiacol HDO; (B) Product distribution of the first and the second bed. Reaction conditions: 1st bed with 0.025 g of Mo<sub>2</sub>C, 2nd bed with 0.3 g of Mo/H-MFI-30-7wt, 350 °C under ambient pressure, propylguaiacol feed of 150  $\mu$ L/h, and 70 mL/min of H<sub>2</sub>.

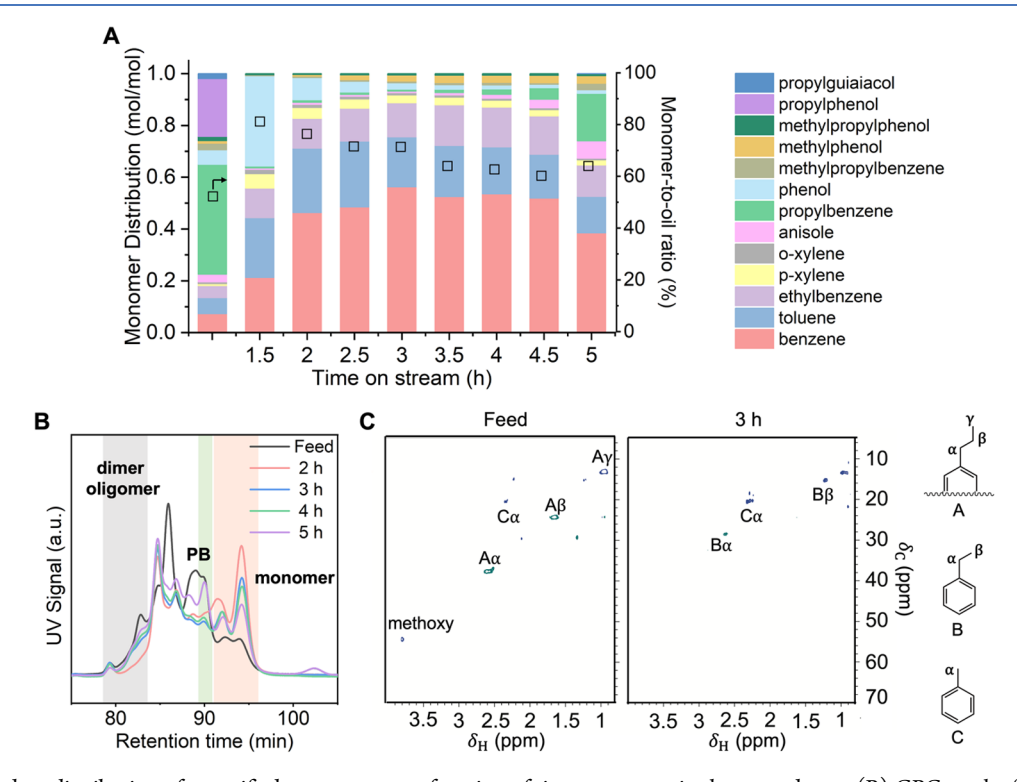


Figure 6. (A) Product distribution of quantified monomers as a function of time on stream in the second pass. (B) GPC on the feed for the second pass and the products collected at different periods of time (PB denotes propylbenzene). (C) HSQC NMR of the feed for the second pass and the product collected at 3 h. Reaction conditions: 1.25 g of Mo/H-MFI-30-7wt diluted with 3.75 g SiC, 375 °C under 900 psi, 90 mL/min  $H_2$ , 0.05 mL/min partial HDO lignin oil, and mesitylene at 1 mL/min for 30 min during start-up.

removal was 119 kJ/mol (Figure 4C), aligning with previous research. The concurrent formation of  $C_3H_8$  and/or  $C_3H_6$  further supports the direct cleavage of the propyl group from the aromatic ring (Figure S19). Notably, this activation energy is substantially higher than those for demethoxylation and dehydroxylation, indicating that C–C bond cleavage is the rate-limiting step when generating platform aromatics from propylguaiacol.

2.4. Catalytic Two-Pass Process to Deoxygenate Lignin Oil into Platform Aromatics. Leveraging the mechanistic insights obtained for the roles of metal/acid sites and the reaction pathway for propylguaiacol hydrodeoxygenation, we implemented a dual-bed system (Figure 5A) to increase the yield of platform aromatics. This system comprised a bed of bulk  $Mo_2C$  (0.025 g) upstream of the

Mo/H-MFI-30-7wt catalyst (0.3 g). Figure 5B shows that the main products from the first bed were propylphenol and propylbenzene, indicating complete  $C_{\rm sp2}$ –OCH<sub>3</sub> bond cleavage by bulk Mo<sub>2</sub>C. These intermediates subsequently entered the second bed, undergoing dehydroxylation and dealkylation on Mo/H-MFI-30-7wt. Notably, our dual-bed system yielded exclusively benzene, toluene, and propylbenzene over 20 h on stream (Figure 5B). The dual bed proved advantageous over the single-bed system, as the initial methoxy group removal by bulk Mo<sub>2</sub>C better preserved the metallic Mo<sub>2</sub>C sites in the Mo/H-MFI-30-7wt catalyst by decreasing the number of oxygenated species in contact with the second bed. This enabled more effective C–O and C–C bond cleavage in propylguaiacol by slowing down deactivation.

These results motivated us to further examine the potential of the bifunctional Mo/H-MFI-30-7wt catalyst for the depolymerization of a real lignin feedstock, whereby the dual-bed system was simulated with a two-pass HDO process using RCF lignin oil from poplar. More specifically, the first pass involved the partial HDO of neat RCF lignin oil with in situ synthesized Mo<sub>2</sub>C via bulk ammonium molybdate tetrahydrate carburization. Figure S20 shows the quantified monomer product distribution over time at 375  $^{\circ}\text{C}$  under 900 psi of hydrogen pressure. This distribution indicates consistent methoxy group removal from the neat RCF lignin oil, leading to the generation of propylphenol, propylbenzene, and their alkylated counterparts. The first pass products were then combined and the aqueous phase was removed to obtain a partially deoxygenated RCF lignin oil containing 52.3% monomers (Figure 6A), which was then fed to a fresh Mo/ H-MFI-30-7wt catalyst bed. Mesitylene was used as a solvent to wet the bed during start-up. The second pass, also conducted at 375 °C, achieved near-complete deoxygenation, as evidenced by the disappearance of propylphenol and propylguaiacol (Figure 6A). The substantial presence of benzene and toluene indicated effective C-O and C-C bond cleavage in lignin-derived compounds from 2 to 4.5 h on stream. It is worth noting that the conversion of the partially deoxygenated RCF oil over Mo/H-MFI-30-7wt increased the total monomer-to-oil ratio to 71.4-81.2% during the first 3 h (Figure 6A). The additional monomer yield relative to those in the process feed indicates that C-C cleavage occurred in the dimers and/or oligomers fractions. This is further supported by the conversion of model dimer bibenzyl over Mo/H-MFI-30-7wt, which exhibited effective C-C bond cleavage, resulting in the steady formation of benzene, toluene, and ethylbenzene (Figure S21). As the reaction proceeded, the monomer-to-oil ratio dropped to ~60% after 5 h on stream. Changes in the molecular weight distribution of the neat lignin oil, the feed for the second pass and the selected products, as characterized by GPC (Figures S22 and 6B), also suggest decreased dimers and oligomer content in the collected products, with a concomitant increase in the UV intensity correlated with monomers during the first 3 h on stream. These results confirm extensive C-C bond cleavage in the dimeric and oligomeric fractions by Mo/ H-MFI-30-7wt. However, precise quantification of these different species remains a significant challenge due to differing UV absorbance for aromatic species. 40,72,73 Rather, comparing HSQC NMR spectra between the feed and the product collected after 3 h supports the occurrence of both C-O and C-C cleavage during the reaction (Figure 6C). Figure S23 displays photographs of neat RCF oil, partial HDO oil, and second pass products, visually representing the extensive HDO achieved by Mo/H-MFI-30-7wt catalyst, marked by a clear solution comprising mainly aromatic species between 2 and 4.5 h, which then gradually shifted to a light red hue due to incomplete phenolic compound removal. Overall, these liquidphase reaction trends corroborate the proposed vapor-phase HDO pathway of propylguaiacol, starting with methoxy group cleavage, followed by successive dehydroxylation and dealkylation. The effective production of aromatics from partially deoxygenated lignin oil highlights the significant potential of the bifunctional Mo/H-MFI-30-7wt catalyst in lignin upgrading.

#### 3. CONCLUSIONS

We developed a bifunctional Mo/H-MFI-30-7wt catalyst to produce platform aromatics, including benzene, toluene, and phenol from lignin-derived monomers. This catalyst enabled the effective cleavage of both C-O and C-C bonds in propylguaiacol. Our findings highlight the importance of the proximity between the metallic Mo<sub>2</sub>C and Brønsted acid sites for tandem deoxygenation and dealkylation, resulting in a high yield of fully deoxygenated aromatics. Achieving an optimal balance between metal and acid sites was essential to effectively deconstruct C-O/C-C bonds and enhance on-stream stability. Insights from the model compound studies were used for depolymerizing real lignin feedstocks into platform aromatics over the bifunctional Mo/H-MFI-30-7wt catalyst using a dual-pass continuous flow system. This work provides a new pathway for the sustainable production of aromatics from lignin-derived monomers and establishes a foundation for the further design of heterogeneous catalysts aimed at upgrading complex lignin feedstocks. Future research will focus on developing bifunctional catalysts and process designs for upgrading more complicated dimeric/oligomeric lignin compounds.

#### 4. MATERIALS AND METHODS

4.1. Materials. For the synthesis of MFI zeolites, colloidal silica (LUDOX LS-30, 30 wt % suspension), aluminum hydroxide (≥99 wt %, Sigma-Aldrich), tetrapropylammonium hydroxide (TPAOH) solution (40 wt % aqueous solution, Merck) and sodium hydroxide (20 wt % aqueous solution, Sigma-Aldrich) were used as provided. 4-Propylguaiacol (≥99 wt %), 4-propylphenol (≥99 wt %) and propylbenzene (≥99 wt %) purchased from Sigma-Aldrich were used provided. Ammonium molybdate tetrahydrate (AMT, ≥99 wt %, Sigma-Aldrich) was used as the molybdenum precursor. Silicon carbide powder (120 grit, ≥98.0%, Alfa Aesar) was used to dilute the catalyst. Quartz chips (fused silicon dioxide, Sigma-Aldrich) were used as an inert packing material to fill reactor dead volume. Ruthenium on carbon (Ru/C, 5 wt %, Sigma-Aldrich) was used as a catalyst to produce lignin oil via reductive catalytic fractionation (RCF). 1,3,5-Tri-tert-butylbenzene (≥98 wt %, TCI) was used as an internal standard for analyzing the products from the liquid-phase reaction.

**4.2. Catalyst Synthesis.** *4.2.1. Synthesis of MFI Zeolite with Different Si/Al Ratios.* Na-MFI zeolites with different Si/Al ratios (130, 75, 30) were synthesized from a gel mixture with a composition of 50 NaOH:  $xAl_2O_3$ :  $300SiO_2$ : 20TPAOH:  $2300H_2O$  (x=1,2,5). First, aluminum hydroxide was dissolved in a solution of 20 wt % NaOH and TPAOH, followed by stirring for 5 min. Subsequently, colloidal silica was incorporated, stirring the mixture for 30 min to ensure homogeneity. The blend was then aged at 90 °C for 16 h. After aging, the mixture was processed in a sealed tubular reactor (stainless steel tube, O.D. 6.6 mm, I.D. 4.4 mm, length 13.5 cm) at 190 °C for 15 min. The solid product was then collected, washed by centrifugation, and dried in an oven at 80 °C overnight.

4.2.2. Preparation of Mo/H-MFI Catalysts. The as-made Na-MFI zeolites were calcined at 550 °C for 8 h to remove the organic structure-directing molecule. The calcined MFI samples were added into a 1 M NH<sub>4</sub>NO<sub>3</sub> aqueous solution with a ratio of 1 g zeolite to 40 mL NH<sub>4</sub>NO<sub>3</sub> solution and stirred at 85 °C for 4 h. Thereafter, the zeolites were recovered

by centrifugation and subjected to another cycle of ion exchange with fresh NH<sub>4</sub>NO<sub>3</sub> solution at 85 °C for 4 h. Subsequently, the zeolites were recovered by filtration, washed, and dried at 80 °C to obtain the NH<sub>4</sub>-form (Si/Al = 130, 75, 30). Another NH<sub>4</sub>-MFI sample with a Si/Al ratio of 11.5 was obtained from Zeolyst International. Finally, the four NH<sub>4</sub>-MFI samples were calcined in air at 550 °C for 3 h with a ramp rate of 2 °C/min to obtain the H-form MFI (H-MFI) zeolites. Mo/H-MFI catalysts were prepared by an impregnation method using a 5 wt % ammonium molybdate tetrahydrate (AMT) solution. The AMT solution was added dropwise to the H-MFI zeolites and mixed with a mortar and pestle. Mo/ H-MFI catalysts with different molybdenum loadings were prepared by varying the volume of AMT solution added to the H-MFI zeolite supports. The homogenized mud-like sample was then dried in an oven at 80 °C overnight. Finally, the solid products were calcined at 550 °C for 5 h with a ramp rate of 2 C/min to obtain the Mo/H-MFI catalysts.

4.2.3. Preparation of Bulk Mo<sub>2</sub>C Catalyst. Mo<sub>2</sub>C was prepared in a custom flow reactor. A 21" long, 1/4" OD Hastelloy reactor tube was heated in a vertically mounted, insulated, single-zone, split furnace (850 W/115 V, Applied Test Systems Series 3210). with steel blocks to ensure adequate heat transfer and maintain isothermal operation. A K-type thermocouple at the middle of the furnace and contacting the outside of the steel blocks was used to regulate temperature with a PID temperature controller (Digi-sense TC9500), while another thermocouple slotted to contact the outside of the reactor tube was used to measure temperature. Gas flow rates were controlled using mass flow controllers (Brooks SLA5850S1BAB1B2A1). AMT was sieved between 60 and 100 mesh and packed into the flow reactor. A quartz wool plug was placed in the bottom of the reactor tube, followed by 9.75" of quartz chips, filling from the bottom of the reactor to the center of the heating zone of the furnace. A quartz wool plug was first loaded, followed by the catalyst bed, and then another quartz wool plug. AMT bed was carburized at 700 °C for 3 h with a ramp rate of 2 °C/min under 15 mL/min CH<sub>4</sub> and 85 mL/min H<sub>2</sub>, followed by a scavenging step to remove the residual coke at 700 °C for 1 h under 85 mL/min H<sub>2</sub>. The reactor was then cooled down to room temperature under hydrogen flow and used for subsequent reactivity studies. For ex situ characterization of carburized samples, they were first passivated in 1% O2 for 2 h prior to removal from the system to eliminate pyrophoricity.

**4.3. Catalyst Characterization.** Powder X-ray diffraction (XRD) patterns were collected over all the solid catalysts using a Bruker D8 diffractometer equipped with a Cu-K $\alpha$  radiation ( $\lambda$  = 1.5418 Å, 40 kV, 40 mA) between 3° and 50° with at a scan rate of 4° min<sup>-1</sup>. The micropore volume and surface area of the catalysts were measured using N<sub>2</sub> adsorption in a Quantachrome Autosorb iQ automated gas sorption system at -196 °C. The micropore volumes were determined by the tplot method. The molybdenum content in the Mo/H-MFI catalysts was determined with an inductively coupled plasmaoptical emission spectrometer (ICP-OES, Agilent 5100) after dissolving the solid products in a hydrofluoric acid solution. Transmission electron microscopy (TEM) images were recorded on an FEI Tecnai microscope at 120 kV. Briefly, 3 mg of the sample was ground and mixed with 5 mL of ethanol. The solution was then sonicated for 20 min, and four to five drops of the dispersed solution were deposited onto a lacey carbon film-supported copper grid (200 mesh). After evaporating the ethanol, the grid was loaded into the microscope and imaged at different magnifications.

Ammonia temperature-programmed desorption (NH<sub>3</sub>-TPD) measurements were conducted in a Micromeritics Autochem II 2920 analyzer equipped with a thermal conductivity detector. 60 mg of catalyst was loaded in a Ushaped quartz reactor between two plugs of quartz wool and pretreated in helium at 500 °C for 30 min. Thereafter, the system was cooled down to 60 °C and ammonia was chemisorbed in three consecutive cycles of saturation with a flow of 50 mL/min of 1 vol % NH<sub>3</sub>/He for 30 min followed by purging with 50 mL/min of helium flow for 30 min. Then the catalyst was heated from 60 to 750 °C at a ramp rate of 5 °C/ min with a flow of 50 mL/min of helium and the desorption of ammonia was monitored with the TCD detector. Temperature-programmed reduction with hydrogen (H2-TPR) was carried out in the same apparatus. Before the measurement, 60 mg of catalyst was treated in helium at 120 °C for 30 min and then cooled to 40 °C. Afterward, the analysis was performed by heating the catalyst to 850  $^{\circ}C$  at 5  $^{\circ}C/min$  with a flow of 50 mL/min of 10 vol % H<sub>2</sub> in Ar, where H<sub>2</sub> consumption was monitored with the TCD detector. Thermogravimetric analysis (TGA) was performed using a TA Instruments Q500 system to quantify the coke formation over the catalyst. The spent catalyst was loaded on a platinum pan and heated from 25 to 800 °C at a ramp rate of 2 °C/min in the presence of air (50 mL/min).

**4.4. Catalytic Activity Measurement.** 4.4.1. HDO of 4-Propylguaiacol. Catalytic activity was measured using a tubular reactor (see preparation of Mo<sub>2</sub>C catalyst) in the vapor phase. Typically, 0.3 g of Mo/H-MFI catalyst (100-140 mesh) was mixed with 1.7 g of silicon carbide (SiC) and packed between quartz chips in a straight Hastelloy reactor. Prior to the reaction, the catalyst was carburized at 700 °C with a ramp rate of 2 °C/min for 3 h under 15 mL/min CH<sub>4</sub> and 85 mL/min H<sub>2</sub>, followed by a scavenging step to remove the residual coke at 700 °C for 1 h under 85 mL/min H<sub>2</sub>. The reactor was then cooled to room temperature under  $H_2$  flow. Next, 4-propylguaiacol was delivered to the bypass line and preheated to 250 °C through capillary tubing connected to a syringe pump (Harvard Apparatus, model 703005) with a flow rate of 150  $\mu$ L/h and then mixed with a separate H<sub>2</sub> flow (70 mL/min STP). The products were analyzed and quantified using an online gas chromatograph (GC) equipped with a mass spectrometer and a flame ionization detector for quantification (FID, Agilent Technologies Model 7890 A). The GC method utilized a split ratio of 100:1, an inlet temperature of 240  $^{\circ}\text{C}$  and a ramp rate of 15  $^{\circ}\text{C/min}$  from 50 to 240 °C followed by a 2 min hold at 240 °C for a total run time of 17 min. The GC was outfitted with a 30 m  $\times$  250  $\mu$ m  $\times$ 0.25 µm Agilent Technologies DB-WAX column. 4-propylguaiacol was tracked until the flow was stabilized. Meanwhile, the reactor was heated to 350 °C with a ramp rate of 5 °C/ min. The feed was switched to the reactor after a stable feed flow was achieved, and the reaction was carried out at 350 °C. Substrate conversion and product selectivity were calculated according to the following definitions, with *n* signifying moles:

Conversion(%)
$$= \frac{n(4-\text{propylguaiacol})_{\text{in}} - n(4-\text{propylguaiacol})_{\text{out}}}{n(4-\text{propylguaiacol})_{\text{in}}} \times 100\%$$
(1)

Selectivity(%)
$$= \frac{n(\text{product})}{n(4-\text{propylguaiacol})_{\text{in}} - n(4-\text{propylguaiacol})_{\text{out}}} \times 100\%$$
(2)

4.4.2. Kinetic Studies. Reaction kinetics measurements were performed under differential conditions with a conversion below 15%. Different intermediates formed during the reaction including 4-propylguaiacol, 4-propylphenol, and propylbenzene were used as feeds to determine potential reaction pathways. The reaction was performed over Mo/H-MFI-30-7wt with a catalyst loading of 30–40 mg. The apparent activation energy for different bond cleavage was measured after the rates had reached a steady state by varying the reaction temperature between 300 and 350 °C.

4.4.3. Liquid-Phase HDO of Real Lignin Oil. RCF lignin oil was generated through the following procedures: in a typical run, 60 g of poplar, 12 g of 5 wt % Ru/C and 400 mL methanol were loaded into a 1 L batch reactor. The reactor was sealed, flushed 3 times with H<sub>2</sub>, and pressurized to 30 bar. The temperature was then ramped to 225 °C for 1.5 h and held for 3 h, during which the mixture was stirred at 700 rpm. After the reaction, the lignin fraction and the solvent were separated by vacuum filtration. The solids were rinsed three times with methanol and the solvent was removed via filtration. The methanol was subsequently removed via rotary evaporation. The resulting oil was purified to remove any sugars or acids that were extracted from the biomass during RCF with a dichloromethane (DCM)/water extraction. Initially, 30 mL of DCM (Laboratory-plus grade, Honeywell) and 30 mL of water (Milli-Q) were used, followed by two rinses of the aqueous phase with 15 mL of DCM. The DCM was removed from the organic phase under vacuum, with a preliminary removal at 100 Torr by rotary evaporation followed by a secondary 0.1 mTorr evacuation on a Schlenk line with magnetic stirring at 100 rpm. Overall, between 7 and 9 g of purified RCF lignin oil was obtained from a single experiment. The oil produced from 5 to 6 batch reactions was combined to generate the neat RCF

The first pass HDO reaction was done as reported previously. 40 Briefly, 5 g of sieved AMT (60-100 mesh) was loaded into the down-flow reactor and carburized in situ with the procedures described above. The reactor was then cooled down to room temperature under hydrogen gas flow prior to the reaction. The steel heat transfer blocks were placed in the furnace and the reactor was slowly pressurized by nitrogen backfill to the reaction pressure of 900 psi. The hydrogen flow rate was set to 90 mL/min and the reactor was heated. Subsequently, toluene flowed at 1 mL/min during heating to prewet the catalyst bed. Once the reactor reached 375 °C, the liquid feed was switched to neat RCF lignin oil flowing at 0.1 mL/min, which was pumped using a Teledyne ISCO syringe pump (Model 500D). Liquid oil was fed into the top of the reactor through a 1/16" OD 316 stainless steel tube which extended to the start of the heating zone. Gas was fed into the top of the reactor via 1/4" OD 316 stainless steel tubing and flowed concurrently with liquid in the down-flow direction through the packed catalyst bed. Liquid samples were collected at room temperature into preweighed vials through a gas/ liquid separator (Jerguson Gage & Valve Co.) every 30 min, which allow for sample mass measurement postexperiment.

The second pass was carried out over the Mo/H-MFI-30-7wt catalyst at 375 °C under 900 psi with a hydrogen flow rate of 90 mL/min. 1.25 g of Mo/H-MFI-30-7wt was diluted with 3.75 g of SiC and packed between quartz chips in the flow reactor. The catalyst was carburized in situ at 700 °C and the reactor was cooled to room temperature thereafter. The products collected during the steady state in the first pass were mixed, followed by a decantation of the aqueous phase to obtain partially deoxygenated RCF lignin oil. The reaction was performed following procedures similar to those for the first pass, but with mesitylene as the solvent to prewet the catalyst bed and a flow of partially deoxygenated RCF oil set at 0.05 mL/min to prevent clogging. The RCF oil feed and the collected samples were analyzed via GC-FID. Typically, 30  $\mu$ L of the sample was dissolved in 2 mL of acetone containing 2 mg/mL of 1,3,5-tri-tert-butylbenzene and injected on GC-FID to quantify monomeric product distribution. The monomer distribution and monomer-to-oil ratio were calculated based on the following equations.

Monomer distribution 
$$\left(\frac{\text{mol}}{\text{mol}}\right) = \frac{n(\text{monomer of interest})}{n(\text{total quantified monomers})}$$
(3)

Monomer-to-oil ratio(%)

$$= \frac{\text{Mass of quantified monomers in GC sample}}{\text{Mass of lignin oil in GC sample}} \times 100\%$$
 (4)

Gel permeation chromatography (GPC) were performed over the feeds and selected products by dissolving the samples in THF at a concentration of 2 mg/mL (HPLC grade, VWR Chemicals BDH) and filtration using a 0.2 µm PTFE syringe filter. 20 µL of each sample was injected using a Hewlett-Packard 1100 series autosampler. Three 5  $\mu$ m PLgel Agilent GPC columns (104, 103, and 50 Å) were arranged in series in order of decreasing pore size. The columns were maintained at a constant temperature of 26 °C, and the system ran at a pressure of approximately 30 bar. A UV diode array detector at a wavelength of 260 nm with a reference wavelength of 360 nm and a 4 nm slit was used to analyze eluents. NMR experiments were used for structural elucidation and assignment authentication for the feeds and the products after the second pass. <sup>1</sup>H-<sup>13</sup>C heteronuclear single quantum coherence (HSQC) NMR spectra were acquired using a Bruker Advance Neo 400 MHz equipped with a 5 mm broad band observe (BBFO) SmartProbe, and the collected spectra were processed using Bruker TopSpin 4.3.0 software. The central solvent peaks (acetone-d<sub>6</sub>) were used as the internal references ( $\delta_c$  = 29.84 ppm,  $\delta_{\rm H}$  = 2.05 ppm). Processing used typical matched Gaussian apodization in F2 (LB = -0.1; GB = 0.001) and squared cosine-bell apodization in F1.

## ASSOCIATED CONTENT

#### Supporting Information

The Supporting Information is available free of charge at https://pubs.acs.org/doi/10.1021/acscatal.5c02259.

XRD patterns,  $N_2$  adsorption—desorption isotherms, TEM images,  $NH_3$ -TPD and  $H_2$ -TPR profiles of Mo/H-MFI catalysts; selectivity of alkylated products formed over Mo/H-MFI catalysts with varied compositions; kinetic studies using key intermediates; and products analysis of the hydrodeoxygenation of RCF oil in the first pass (PDF)

#### AUTHOR INFORMATION

# **Corresponding Authors**

Gregg T. Beckham — Renewable Resources and Enabling Sciences Center, National Renewable Energy Laboratory, Golden, Colorado 80401, United States; Center for Bioenergy Innovation, Oak Ridge, Tennessee 37831, United States; orcid.org/0000-0002-3480-212X;

Email: gregg.beckham@nrel.gov

Yuriy Román-Leshkov — Department of Chemical Engineering, Massachusetts Institute of Technology, Cambridge, Massachusetts 02139, United States; orcid.org/0000-0002-0025-4233; Email: yroman@

#### **Authors**

mit.edu

Jie Zhu – Department of Chemical Engineering, Massachusetts Institute of Technology, Cambridge, Massachusetts 02139, United States

Matthew S. Webber – Department of Chemical Engineering, Massachusetts Institute of Technology, Cambridge, Massachusetts 02139, United States

Jamison Watson – Department of Chemical Engineering, Massachusetts Institute of Technology, Cambridge, Massachusetts 02139, United States

Complete contact information is available at: https://pubs.acs.org/10.1021/acscatal.5c02259

#### **Notes**

The authors declare no competing financial interest.

#### ACKNOWLEDGMENTS

The work was partially funded by the Center for Bioenergy Innovation (CBI), U.S. Department of Energy, Office of Science, Biological and Environmental Research Program under Award Number ERKP886. J.W. acknowledges the financial support by the Schmidt Science Fellows program, in partnership with the Rhodes Trust. This work was partially authored by the National Renewable Energy Laboratory for the U.S. Department of Energy (DOE) under Contract No. DE-AC36-08GO28308. We acknowledge partial funding from the U.S. DOE Office of Energy Efficiency and Renewable Energy Bioenergy Technologies Office. The views expressed in the article do not necessarily represent the views of the DOE or the U.S. Government.

## REFERENCES

- (1) Zakzeski, J.; Bruijnincx, P. C. A.; Jongerius, A. L.; Weckhuysen, B. M. The Catalytic Valorization of Lignin for the Production of Renewable Chemicals. *Chem. Rev.* **2010**, *110* (6), 3552–3599.
- (2) Li, C.; Zhao, X.; Wang, A.; Huber, G. W.; Zhang, T. Catalytic Transformation of Lignin for the Production of Chemicals and Fuels. *Chem. Rev.* **2015**, *115* (21), 11559–11624.
- (3) Dong, L.; Lin, L.; Han, X.; Si, X.; Liu, X.; Guo, Y.; Lu, F.; Rudić, S.; Parker, S. F.; Yang, S.; et al. Breaking the Limit of Lignin Monomer Production via Cleavage of Interunit Carbon-Carbon Linkages. *Chem.* **2019**, *5* (6), 1521–1536.
- (4) Xu, C.; Arancon, R. A. D.; Labidi, J.; Luque, R. Lignin depolymerisation strategies: towards valuable chemicals and fuels. *Chem. Soc. Rev.* **2014**, *43* (22), 7485–7500.
- (5) Liao, Y.; Zhong, R.; d'Halluin, M.; Verboekend, D.; Sels, B. F. Aromatics Production from Lignocellulosic Biomass: Shape Selective Dealkylation of Lignin-Derived Phenolics over Hierarchical ZSM-5. ACS Sustain. Chem. Eng. 2020, 8 (23), 8713–8722.

- (6) Haveren, J. v.; Scott, E. L.; Sanders, J. Bulk Chemicals from Biomass. *Biofuel Bioprod Bior.* **2008**, 2 (1), 41–57.
- (7) Bertella, S.; Luterbacher, J. S. Lignin Functionalization for the Production of Novel Materials. *Trends Chem.* **2020**, *2* (5), 440–453.
- (8) Jacobs, P. A.; Dusselier, M.; Sels, B. F. Will Zeolite-Based Catalysis be as Relevant in Future Biorefineries as in Crude Oil Refineries? *Angew. Chem., Int. Ed.* **2014**, *53* (33), 8621–8626.
- (9) Upton, B. M.; Kasko, A. M. Strategies for the Conversion of Lignin to High-Value Polymeric Materials: Review and Perspective. *Chem. Rev.* **2016**, *116* (4), 2275–2306.
- (10) Schutyser, W.; Renders, T.; Van den Bosch, S.; Koelewijn, S. F.; Beckham, G. T.; Sels, B. F. Chemicals from Lignin: An Interplay of Lignocellulose Fractionation, Depolymerisation, and Upgrading. *Chem. Soc. Rev.* **2018**, *47* (3), 852–908.
- (11) Zhang, C.; Wang, F. Catalytic Lignin Depolymerization to Aromatic Chemicals. *Acc. Chem. Res.* **2020**, 53 (2), 470–484.
- (12) Alherech, M.; Omolabake, S.; Holland, C. M.; Klinger, G. E.; Hegg, E. L.; Stahl, S. S. From Lignin to Valuable Aromatic Chemicals: Lignin Depolymerization and Monomer Separation via Centrifugal Partition Chromatography. ACS Cent. Sci. 2021, 7 (11), 1831–1837.
- (13) Wu, X.; Liao, Y.; Bomon, J.; Tian, G.; Bai, S.-T.; Van Aelst, K.; Zhang, Q.; Vermandel, W.; Wambacq, B.; Maes, B. U. W.; Yu, J.; Sels, B. F. Lignin-First Monomers to Catechol: Rational Cleavage of C–O and C–C Bonds over Zeolites. *ChemSusChem* **2022**, *15* (7), No. e202102248.
- (14) Luo, Z.; Liu, C.; Radu, A.; de Waard, D. F.; Wang, Y.; Behaghel de Bueren, J. T.; Kouris, P. D.; Boot, M. D.; Xiao, J.; Zhang, H.; Xiao, R.; Luterbacher, J. S.; Hensen, E. J. M. Carbon-Carbon Bond Cleavage for a Lignin Refinery. *Nat. Chem. Eng.* **2024**, *1* (1), 61–72. (15) Zhao, C.; Kou, Y.; Lemonidou, A. A.; Li, X.; Lercher, J. A. Highly Selective Catalytic Conversion of Phenolic Bio-Oil to Alkanes. *Angew. Chem., Int. Ed.* **2009**, *48* (22), 3987–3990.
- (16) Yan, N.; Yuan, Y.; Dykeman, R.; Kou, Y.; Dyson, P. J. Hydrodeoxygenation of Lignin-Derived Phenols into Alkanes by Using Nanoparticle Catalysts Combined with Brønsted Acidic Ionic Liquids. *Angew. Chem., Int. Ed.* **2010**, 49 (32), 5549–5553.
- (17) Jongerius, A. L.; Bruijnincx, P. C. A.; Weckhuysen, B. M. Liquid-Phase Reforming and Hydrodeoxygenation as a Two-Step Route to Aromatics from Lignin. *Green Chem.* **2013**, *15* (11), 3049–
- (18) Saidi, M.; Samimi, F.; Karimipourfard, D.; Nimmanwudipong, T.; Gates, B. C.; Rahimpour, M. R. Upgrading of Lignin-Derived Bio-Oils by Catalytic Hydrodeoxygenation. *Energy Environ. Sci.* **2014**, *7* (1), 103–129.
- (19) Nelson, R. C.; Baek, B.; Ruiz, P.; Goundie, B.; Brooks, A.; Wheeler, M. C.; Frederick, B. G.; Grabow, L. C.; Austin, R. N. Experimental and Theoretical Insights into the Hydrogen-Efficient Direct Hydrodeoxygenation Mechanism of Phenol over Ru/TiO<sub>2</sub>. ACS Catal. **2015**, *5* (11), 6509–6523.
- (20) Robinson, A. M.; Hensley, J. E.; Medlin, J. W. Bifunctional Catalysts for Upgrading of Biomass-Derived Oxygenates: A Review. ACS Catal. 2016, 6 (8), 5026–5043.
- (21) Teles, C. A.; Rabelo-Neto, R. C.; de Lima, J. R.; Mattos, L. V.; Resasco, D. E.; Noronha, F. B. The Effect of Metal Type on Hydrodeoxygenation of Phenol Over Silica Supported Catalysts. *Catal. Lett.* **2016**, *146* (10), 1848–1857.
- (22) Ma, D.; Lu, S.; Liu, X.; Guo, Y.; Wang, Y. Depolymerization and Hydrodeoxygenation of Lignin to Aromatic Hydrocarbons with a Ru Catalyst on a Variety of Nb-Based Supports. *Chin. J. Catal.* **2019**, 40 (4), 609–617.
- (23) Kim, S.; Kwon, E. E.; Kim, Y. T.; Jung, S.; Kim, H. J.; Huber, G. W.; Lee, J. Recent Advances in Hydrodeoxygenation of Biomass-Derived Oxygenates over Heterogeneous Catalysts. *Green Chem.* **2019**, *21* (14), 3715–3743.
- (24) Wang, X.; Arai, M.; Wu, Q.; Zhang, C.; Zhao, F. Hydrodeoxygenation of Lignin-Derived Phenolics A Review on the Active Sites of Supported Metal Catalysts. *Green Chem.* **2020**, 22 (23), 8140–8168.

- (25) Gutierrez, A.; Kaila, R. K.; Honkela, M. L.; Slioor, R.; Krause, A. O. I. Hydrodeoxygenation of Guaiacol on Noble Metal Catalysts. *Catal. Today* **2009**, *147* (3), 239–246.
- (26) Zhao, C.; He, J.; Lemonidou, A. A.; Li, X.; Lercher, J. A. Aqueous-Phase Hydrodeoxygenation of Bio-Derived Phenols to Cycloalkanes. *J. Catal.* **2011**, 280 (1), 8–16.
- (27) Güvenatam, B.; Kurşun, O.; Heeres, E. H. J.; Pidko, E. A.; Hensen, E. J. M. Hydrodeoxygenation of Mono- and Dimeric Lignin Model Compounds on Noble Metal Catalysts. *Catal. Today* **2014**, 233, 83–91.
- (28) Bui, V. N.; Laurenti, D.; Afanasiev, P.; Geantet, C. Hydrodeoxygenation of Guaiacol with CoMo Catalysts. Part I: Promoting Effect of Cobalt on HDO Selectivity and Activity. *Appl. Catal. B: Environ.* **2011**, *101* (3), 239–245.
- (29) Zhao, H. Y.; Li, D.; Bui, P.; Oyama, S. T. Hydrodeoxygenation of Guaiacol as Model Compound for Pyrolysis Oil on Transition Metal Phosphide Hydroprocessing Catalysts. *Appl. Catal. A: Gen.* **2011**, 391 (1), 305–310.
- (30) Chen, W.; Maugé, F.; van Gestel, J.; Nie, H.; Li, D.; Long, X. Effect of Modification of the Alumina Acidity on the Properties of Supported Mo and CoMo Sulfide Catalysts. *J. Catal.* **2013**, 304, 47–62.
- (31) Osorio Velasco, J.; van der Linden, I.; Deuss, P. J.; Heeres, H. J. Efficient Depolymerization of Lignins to Alkylphenols Using Phosphided NiMo Catalysts. *Catal. Sci. Technol.* **2021**, *11* (15), 5158–5170.
- (32) Wu, K.; Wang, W.; Guo, H.; Yang, Y.; Huang, Y.; Li, W.; Li, C. Engineering Co Nanoparticles Supported on Defect MoS<sub>2-x</sub> for Mild Deoxygenation of Lignin-Derived Phenols to Arenes. *ACS Energy Lett.* **2020**, 5 (4), 1330–1336.
- (33) Diao, X.; Ji, N.; Li, X.; Rong, Y.; Zhao, Y.; Lu, X.; Song, C.; Liu, C.; Chen, G.; Ma, L.; Wang, S.; Liu, Q.; Li, C. Fabricating High Temperature Stable Mo-Co<sub>9</sub>S<sub>8</sub>/Al<sub>2</sub>O<sub>3</sub> Catalyst for Selective Hydrodeoxygenation of Lignin to Arenes. *Appl. Catal. B: Environ.* **2022**, 305, No. 121067.
- (34) Jia, Z.; Ji, N.; Diao, X.; Li, X.; Zhao, Y.; Lu, X.; Liu, Q.; Liu, C.; Chen, G.; Ma, L.; et al. Highly Selective Hydrodeoxygenation of Lignin to Naphthenes over Three-Dimensional Flower-like Ni<sub>2</sub>P Derived from Hydrotalcite. *ACS Catal.* **2022**, *12* (2), 1338–1356.
- (35) Wang, W.; Xiao, T.; Wang, D.; Yang, H.; Qiang, Q.; Shen, Z.; Yang, Y.; Wu, K.; Li, C. Scale-Up Foreseeable Fabrication of CoS-MoS<sub>2</sub> for Efficient Deoxygenation of Lignin-Derived Phenolics to Arenes. ACS Catal. 2023, 13 (13), 8792–8802.
- (36) Ren, H.; Yu, W.; Salciccioli, M.; Chen, Y.; Huang, Y.; Xiong, K.; Vlachos, D. G.; Chen, J. G. Selective Hydrodeoxygenation of Biomass-Derived Oxygenates to Unsaturated Hydrocarbons using Molybdenum Carbide Catalysts. *ChemSusChem* **2013**, *6* (5), 798–801.
- (37) Lee, W.-S.; Wang, Z.; Wu, R. J.; Bhan, A. Hydrodeoxygenation of Anisole to Benzene on Molybdenum Carbide Catalysts. *J. Catal.* **2014**, *319*, 44–53.
- (38) Sullivan, M. M.; Held, J. T.; Bhan, A. Structure and site evolution of molybdenum carbide catalysts upon exposure to oxygen. *J. Catal.* **2015**, 326, 82–91.
- (39) Lee, W.-S.; Kumar, A.; Wang, Z.; Bhan, A. Chemical Titration and Transient Kinetic Studies of Site Requirements in  $Mo_2C$ -Catalyzed Vapor Phase Anisole Hydrodeoxygenation. *ACS Catal.* **2015**, 5 (7), 4104-4114.
- (40) Stone, M. L.; Webber, M. S.; Mounfield, W. P.; Bell, D. C.; Christensen, E.; Morais, A. R. C.; Li, Y.; Anderson, E. M.; Heyne, J. S.; Beckham, G. T.; Román-Leshkov, Y. Continuous Hydrodeoxygenation of Lignin to Jet-Range Aromatic Hydrocarbons. *Joule* **2022**, *6* (10), 2324–2337.
- (41) Song, W.; Liu, Y.; Baráth, E.; Zhao, C.; Lercher, J. A. Synergistic Effects of Ni and Acid Sites for Hydrogenation and C-O Bond Cleavage of Substituted Phenols. *Green Chem.* **2015**, *17* (2), 1204–1218.
- (42) Foo, G. S.; Rogers, A. K.; Yung, M. M.; Sievers, C. Steric Effect and Evolution of Surface Species in the Hydrodeoxygenation of Bio-

- Oil Model Compounds over Pt/HBEA. ACS Catal. 2016, 6 (2), 1292–1307.
- (43) Wang, M.; Lu, J.; Zhang, X.; Li, L.; Li, H.; Luo, N.; Wang, F. Two-Step, Catalytic C-C Bond Oxidative Cleavage Process Converts Lignin Models and Extracts to Aromatic Acids. *ACS Catal.* **2016**, *6* (9), 6086–6090.
- (44) Verboekend, D.; Liao, Y.; Schutyser, W.; Sels, B. F. Alkylphenols to Phenol and Olefins by Zeolite Catalysis: A Pathway to Valorize Raw and Fossilized Lignocellulose. *Green Chem.* **2016**, *18* (1), 297–306.
- (45) Wang, Y.; Wang, Q.; He, J.; Zhang, Y. Highly Effective C-C Bond Cleavage of Lignin Model Compounds. *Green Chem.* **2017**, *19* (13), 3135–3141.
- (46) Liu, H.; Li, H.; Lu, J.; Zeng, S.; Wang, M.; Luo, N.; Xu, S.; Wang, F. Photocatalytic Cleavage of C-C Bond in Lignin Models under Visible Light on Mesoporous Graphitic Carbon Nitride through  $\pi$ – $\pi$  Stacking Interaction. *ACS Catal.* **2018**, 8 (6), 4761–4771.
- (47) Guadix-Montero, S.; Sankar, M. Review on Catalytic Cleavage of C-C Inter-unit Linkages in Lignin Model Compounds: Towards Lignin Depolymerisation. *Top. Catal.* **2018**, *61* (3), 183–198.
- (48) Subbotina, E.; Rukkijakan, T.; Marquez-Medina, M. D.; Yu, X.; Johnsson, M.; Samec, J. S. M. Oxidative cleavage of C-C bonds in lignin. *Nat. Chem.* **2021**, *13* (11), 1118–1125.
- (49) Gu, N. X.; Palumbo, C. T.; Bleem, A. C.; Sullivan, K. P.; Haugen, S. J.; Woodworth, S. P.; Ramirez, K. J.; Kenny, J. K.; Stanley, L. D.; Katahira, R.; Stahl, S. S.; Beckham, G. T. Autoxidation Catalysis for Carbon-Carbon Bond Cleavage in Lignin. *ACS Cent. Sci.* **2023**, 9 (12), 2277–2285.
- (50) Palumbo, C. T.; Gu, N. X.; Bleem, A. C.; Sullivan, K. P.; Katahira, R.; Stanley, L. M.; Kenny, J. K.; Ingraham, M. A.; Ramirez, K. J.; Haugen, S. J.; Amendola, C. R.; Stahl, S. S.; Beckham, G. T. Catalytic Carbon-Carbon Bond Cleavage in Lignin via Manganese—Zirconium-Mediated Autoxidation. *Nat. Commun.* **2024**, *15* (1), 862.
- (51) Li, K.; Wang, R.; Chen, J. Hydrodeoxygenation of Anisole over Silica-Supported Ni<sub>2</sub>P, MoP, and NiMoP Catalysts. *Energy Fuels* **2011**, 25 (3), 854–863.
- (52) Shao, Y.; Xia, Q.; Dong, L.; Liu, X.; Han, X.; Parker, S. F.; Cheng, Y.; Daemen, L. L.; Ramirez-Cuesta, A. J.; Yang, S.; Wang, Y. Production of Arenes via Direct Lignin Ipgrading over a Niobium-Based Catalyst. *Nat. Commun.* **2017**, *8* (1), 16104.
- (53) Liao, Y.; d'Halluin, M.; Makshina, E.; Verboekend, D.; Sels, B. F. Shape Selectivity Vapor-Phase Conversion of Lignin-Derived 4-Ethylphenol to Phenol and Ethylene over Acidic Aluminosilicates: Impact of Acid Properties and Pore Constraint. *Appl. Catal. B: Environ.* **2018**, 234, 117–129.
- (54) Liao, Y.; Zhong, R.; Makshina, E.; d'Halluin, M.; van Limbergen, Y.; Verboekend, D.; Sels, B. F. Propylphenol to Phenol and Propylene over Acidic Zeolites: Role of Shape Selectivity and Presence of Steam. ACS Catal. 2018, 8 (9), 7861–7878.
- (55) Huang, X.; Ludenhoff, J. M.; Dirks, M.; Ouyang, X.; Boot, M. D.; Hensen, E. J. M. Selective Production of Biobased Phenol from Lignocellulose-Derived Alkylmethoxyphenols. *ACS Catal.* **2018**, 8 (12), 11184–11190.
- (56) Zhang, W.; Chen, J.; Liu, R.; Wang, S.; Chen, L.; Li, K. Hydrodeoxygenation of Lignin-Derived Phenolic Monomers and Dimers to Alkane Fuels over Bifunctional Zeolite-Supported Metal Catalysts. ACS Sustain. Chem. Eng. 2014, 2 (4), 683–691.
- (57) Meng, Q.; Yan, J.; Wu, R.; Liu, H.; Sun, Y.; Wu, N.; Xiang, J.; Zheng, L.; Zhang, J.; Han, B. Sustainable Production of Benzene from Lignin. *Nat. Commun.* **2021**, *12* (1), 4534.
- (58) Prasomsri, T.; Shetty, M.; Murugappan, K.; Román-Leshkov, Y. Insights into the Catalytic Activity and Surface Modification of MoO<sub>3</sub> during the Hydrodeoxygenation of Lignin-Derived Model Compounds into Aromatic Hydrocarbons under Low Hydrogen Pressures. *Energy Environ. Sci.* **2014**, *7* (8), 2660–2669.
- (59) Chen, C.-J.; Lee, W.-S.; Bhan, A. Mo<sub>2</sub>C Catalyzed Vapor Phase Hydrodeoxygenation of Lignin-Derived Phenolic Compound Mix-

tures to Aromatics under Ambient Pressure. Appl. Catal. A: Gen. 2016, 510, 42-48.

- (60) Sullivan, M. M.; Bhan, A. Acetone Hydrodeoxygenation over Bifunctional Metallic-Acidic Molybdenum Carbide Catalysts. *ACS Catal.* **2016**, 6 (2), 1145–1152.
- (61) Kumar, A.; Bhan, A. Oxygen Content as A Variable to Control Product Selectivity in Hydrodeoxygenation Reactions on Molybdenum Carbide Catalysts. *Chem. Eng. Sci.* **2019**, *197*, *371*–*378*.
- (62) Zhang, J.; Lombardo, L.; Gözaydın, G.; Dyson, P. J.; Yan, N. Single-Step Conversion of Lignin Monomers to Phenol: Bridging the Gap between Lignin and High-Value Chemicals. *Chin. J. Catal.* **2018**, 39 (9), 1445–1452.
- (63) Tessonnier, J.-P.; Louis, B.; Rigolet, S.; Ledoux, M. J.; Pham-Huu, C. Methane Dehydro-aromatization on Mo/ZSM-5: About the Hidden Role of Brønsted Acid Sites. *Appl. Catal. A: Gen.* **2008**, 336 (1), 79–88.
- (64) Mannei, E.; Ayari, F.; Asedegbega-Nieto, E.; Mhamdi, M.; Delahay, G.; Ksibi, Z.; Ghorbel, A. Physicochemical and Catalytic Properties of Over- and Low-Exchanged Mo-ZSM-5 Ammoxidation Catalysts. *Chem. Pap.* **2019**, *73* (3), 619–633.
- (65) Ghanbari, B.; Kazemi Zangeneh, F.; Taheri Rizi, Z.; Aghaei, E. High-Impact Promotional Effect of Mo Impregnation on Aluminum-Rich and Alkali-Treated Hierarchical Zeolite Catalysts on Methanol Aromatization. ACS Omega 2020, 5 (21), 11971–11986.
- (66) Bond, G. C.; Tahir, S. F. Structure and Reactivity of Titania-Supported Oxides: V. Influence of Phosphorus and Potassium Impurities on the Properties of Molybdenum Oxide Supported on Titania. *Appl. Catal. A: Gen.* **1993**, *105* (2), 281–288.
- (67) Liu, H.; Xu, Y. H<sub>2</sub>-TPR Study on Mo/HZSM-5 Catalyst for CH<sub>4</sub> Dehydroaromatization. *Chin. J. Catal.* **2006**, 27 (4), 319–323.
- (68) Ma, D.; Shu, Y.; Bao, X.; Xu, Y. Methane Dehydro-aromatization under Nonoxidative Conditions over Mo/HZSM-5 Catalysts: EPR Study of the Mo Species on/in the HZSM-5 Zeolite. *J. Catal.* **2000**, 189 (2), 314–325.
- (69) Song, S.; Zhang, J.; Yan, N. Support Effects in the De-Methoxylation of Lignin Monomer 4-Propylguaiacol over Molybdenum-Based Catalysts. *Fuel Process. Technol.* **2020**, *199*, No. 106224.
- (70) Ghampson, I. T.; Canales, R.; Escalona, N. A Study of the Hydrodeoxygenation of Anisole over Re-MoO<sub>x</sub>/TiO<sub>2</sub> Catalyst. *Appl. Catal. A: Gen.* **2018**, 549, 225–236.
- (71) Shetty, M.; Anderson, E. M.; Green, W. H.; Román-Leshkov, Y. Kinetic Analysis and Reaction Mechanism for Anisole Conversion over Zirconia-Supported Molybdenum Oxide. *J. Catal.* **2019**, *376*, 248–257.
- (72) Van Aelst, K.; Van Sinay, E.; Vangeel, T.; Cooreman, E.; Van den Bossche, G.; Renders, T.; Van Aelst, J.; Van den Bosch, S.; Sels, B. F. Reductive Catalytic Fractionation of Pine Wood: Elucidating and Quantifying the Molecular Structures in the Lignin Oil. *Chem. Sci.* **2020**, *11* (42), 11498–11508.
- (73) Dao Thi, H.; Van Aelst, K.; Van den Bosch, S.; Katahira, R.; Beckham, G. T.; Sels, B. F.; Van Geem, K. M. dentification and Quantification of Lignin Monomers and Oligomers from Reductive Catalytic Fractionation of Pine Wood with GC × GC FID/MS. *Green Chem.* **2022**, 24 (1), 191–206.



CAS BIOFINDER DISCOVERY PLATFORM™

# BRIDGE BIOLOGY AND CHEMISTRY FOR FASTER ANSWERS

Analyze target relationships, compound effects, and disease pathways

**Explore the platform** 

